Katoh *et al. Earth, Planets and Space (2018) 70:149*
https://doi.org/10.1186/s40623-018-0921-6

Earth, Planets and Space

EXPRESS LETTER

Open Access

The relationship between S-wave reflectors and deep low-frequency earthquakes in the northern Kinki district, southwestern Japan

Shinya Katoh*, Yoshihisa Iio, Hiroshi Katao, Masayo Sawada, Kazuhide Tomisaka, Tsutomu Miura and Itaru Yoneda

Abstract

We conducted high-resolution reflection analysis of data from 168 seismic stations with an average spacing of about 5 km, in northern Kinki district, southwestern Japan. Reflection analysis has previously been conducted in this region, assuming a homogeneous horizontal structure, resulting in an inclined planar zone of high relative reflection strengths (S-wave reflector). However, if the reflector is actually inclined, the location of the S-wave reflector differs from that of an assumed homogeneous horizontal structure. Hence, this study conducted high-resolution reflection analysis to determine the accurate location of the S-wave reflector. We confirm the previously reported S-wave reflector (reflector W). Furthermore, we detected the accurate location of the S-wave reflector and obtained more detailed results that revealed a second S-wave reflection structure (reflector E) to the east of reflector W, in an area that has not be imaged by previous studies. The northern edges of reflector E and reflector W are located near different hypocentral areas of deep low-frequency earthquakes (DLFs). Reflector W exists along the Kyoto Nishiyama fault zone, and its position appears to change along the fault zone as it deepens. Similarly, reflector E exists along the Hanaore and Biwako Seigan fault zones and its position appears to change along these fault zones. The reflector W and reflector E are imaged as separate S-wave reflectors in deeper regions, but they coalesce in shallower regions. According to previous studies, crustal fluid by dehydration from the Philippine Sea plate exists near these epicenters and we infer that this crustal fluid causes DLFs and forms S-wave reflectors.

Keywords: Reflection analysis, Lower crust, Fluid, Niigata–Kobe Tectonic Zone, Deep low-frequency earthquakes, Manten system

Introduction

Beneath the island arc of southwestern Japan, the Philippine Sea plate subducts to the northwest (Hirose et al. 2008) (Fig. 1a). Various interesting phenomena occur at this boundary, such as non-volcanic deep low-frequency earthquakes (DLFs) (Obara 2002). DLFs are categorized based on their location, and the DLFs that are located far from plate boundaries and active volcanoes are isolated intraplate DLFs (Aso et al. 2012). Isolated interplate DLFs often occur in the northern Kinki district, where these are isolated intraplate DLFs, as there are no active volcanoes.

This area is part of the Niigata–Kobe Tectonic Zone (NKTZ), identified as a zone with high strain rates (Sagiya et al. 2000). Iio et al. (2002) proposed the water-weakened lower crust model, which explains that strain rates are high in the NKTZ. According to Iio et al. (2002), the lower crust was weakened by accumulating fluid rose from the mantle. Therefore, deformation concentrated at the NKTZ, and the strain rate observed at the surface was increased.

*Correspondence: katou.shinya.28z@st.kyoto-u.ac.jp
Graduate School of Science, Kyoto University, Gokasho, Uji City, Kyoto 611-0011, Japan

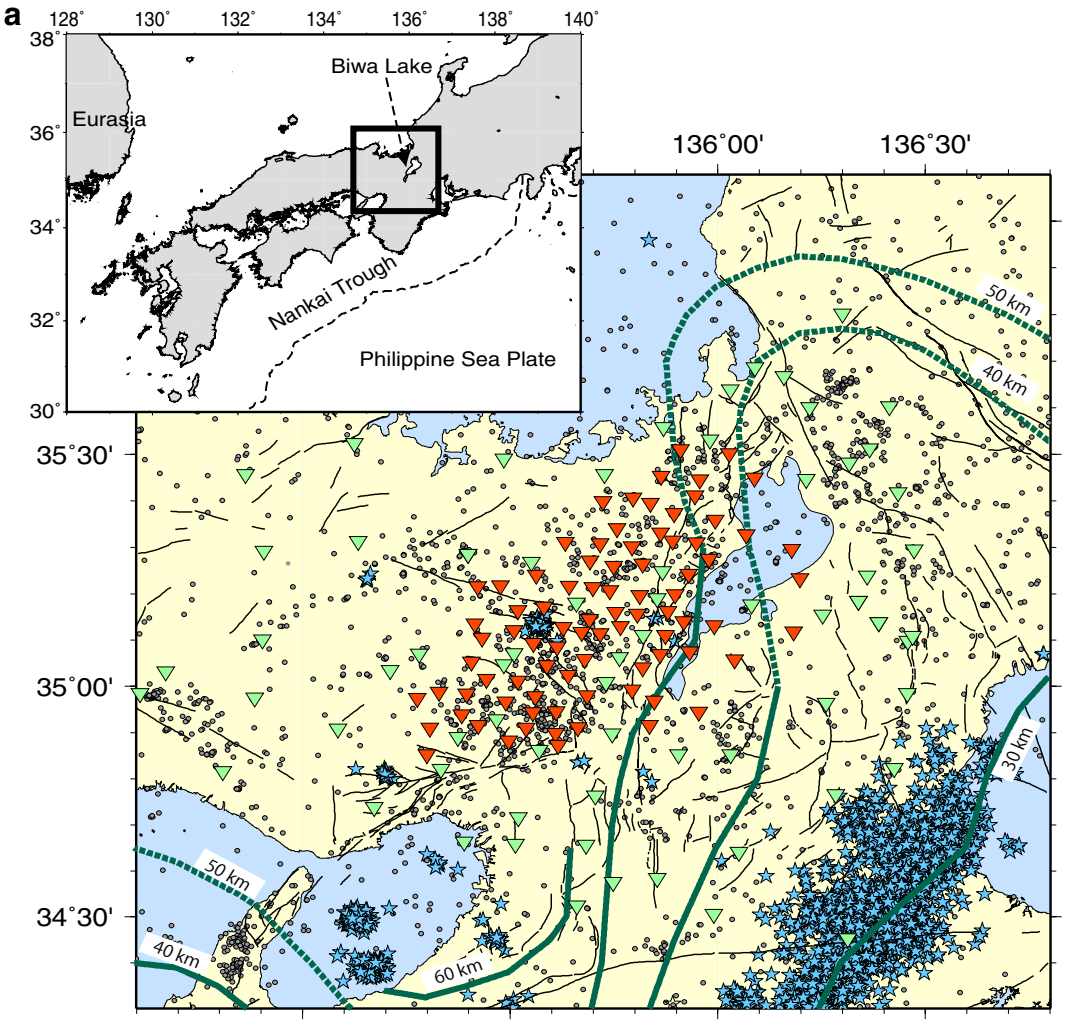
a
128°
130°
132°
134°
136°
138°
140°
38°
36°
34°
32°
30°
Biwa Lake
Eurasia
Nankai Trough
Philippine Sea Plate
136°00'
136°30'
35°30'
35°00'
34°30'
50 km
40 km
30 km
60 km
b
2010/3/8 5:11:46+0900 (JST)
DP.YGI
Transverse component
direct S-wave
direct P-wave
reflection wave
Amplitude(μm/s)
5
0
-5
0
10
20
30
Time(s)

(See figure on previous page.)
Fig. 1 Seismic stations and hypocenters used in this study and example of waveform on transverse component at DP.YGI. **a** Gray dots represent hypocenters. Red and green triangles represent temporary and permanent seismic stations, respectively, of Kyoto University, AIST, NIED, and JMA. Blue stars represent hypocenters of deep low-frequency earthquakes (DLFs). Black lines indicate the location of active faults. Green lines show the depth contours of the upper boundary of the Philippine Sea plate reported by Hirose et al. (2008). **b** In the inset map, the black star and circle represent the hypocenter of a M2.0 earthquake on March 8, 2010, and seismic station (DP.YGI), respectively. This waveform is unfiltered by a 5–8-Hz band-pass filter

Microearthquake activity occurs continuously in this district, in particular to the north of the Arima–Takatsuki Tectonic Line (Iio 1996). Waveforms of microearthquakes that occur in this district show distinct reflected S-waves (Katao 2002) (Fig. 1b). Katao et al. (2007) conducted reflection analysis and estimated the distribution of S-wave reflection points using data observed at 10 permanent stations. They found a planar distribution of S-wave reflection points inclining northward at a depth of 20–30 km, but the detailed shape of the S-wave reflector was unknown. Aoki et al. (2016) conducted high-resolution analysis using data from 128 seismic stations with an average spacing of about 5 km and found that the S-wave reflector was inclined to the north, and that isolated intraplate DLFs occur near the edge of the S-wave reflector. The relationship between DLFs and fluid has been previously studied (Ohami and Obara 2002), and Aoki et al. (2016) proposed that the reflector is the fluid path, and that isolated intraplate DLFs are related to the fluid.

Aoki et al. (2016) conducted reflection analysis, assuming a homogeneous horizontal structure, but in the current study the estimated S-wave reflector is inclined. If the true reflector is inclined, then true locations of reflection points will differ from those obtained assuming a homogeneous horizontal structure, since locations of reflection points will differ from those obtained assuming a homogeneous horizontal structure. Hence, the purpose of this study is to detect the accurate location of the S-wave reflector using a modified version of the method of Aoki et al. (2016) investigating the relationship between the inclined S-wave reflector and DLFs.

Data and method

In this study, we used waveforms from 168 seismic stations, 61 of which are permanent and 107 are temporary. The temporary seismic stations have been operating since 2009, using a next-generation seismometer system called the "Manten system," which has a sampling frequency of 250 Hz (Miura et al. 2010; Iio 2011). We used earthquakes of magnitude (M) greater than 2.0 that occurred in this area between February 2009 and December 2013. We modified the method used by Aoki et al. (2016) and conducted high-resolution reflection analysis considering the effect of an inclined S-wave reflector.

In this analysis, we converted the two horizontal components to the transverse direction and applied a 5–8-Hz band-pass filter to match the dominant frequency of the reflected wave. We corrected amplitudes by the attenuation factor Q_C of coda waves and applied coda normalization (Aki 1980) to correct relative reflection strengths. We derived Q_C in a window 25–28 s after the origin time, because the seismic waveforms did not include large phase and we do not use the seismic waveforms that direct S-wave is included in window 25–28 s. Next, we conducted normal move-out correction (NMO) (Inamori et al. 1992) assuming an S-wave velocity of 3.5 km/s. However, a single velocity resulted in depth errors when we carried out depth conversion. Hence, we used the root-mean-square S-wave velocity (V_{RMS}) of the JMA2001 velocity structure (Ueno et al. 2002) to determine the depth error. The V_{RMS} between the ground surface and a depth of 34 km, corresponding to the lower end of the S-wave reflector, is calculated as 3.661 km/s, and the V_{RMS} between the ground surface and a depth of 22 km, corresponding to the upper end of the S-wave reflector, is calculated as 3.502 km/s. From these results, we estimated the depth error to be about 0.002 km at the upper end of the S-wave reflector and at about 1.61 km at the lower end of the S-wave reflector, when the travel time is 20 s. Because both the depth errors and the velocity differences from V_{RMS} for the reflectors at the depths of 22 km and 34 km are small, we think that a simplified S-wave velocity structure with a constant value of 3.5 km/s is appropriate.

To detect the three-dimensional distribution of relative reflection strengths, we used the three-dimensional stacking method (Doi and Nishigami 2007) and set X-, Y-, and Z-axes as latitude, longitude, and vertical directions, respectively. The size of the study area is 300 km along the X-axis, 300 km along the Y-axis, and 60 km along the Z-axis. We set the origin of the coordinates as the point (35.2°N, 135.7°E). The area was divided into 2,400,000 grid cells with an interval of 1.5 km along the X- and Y-axes and 1 km along the Z-axis. We detected the relative reflection strength for each grid cell, following the method of Aoki et al. (2016).

The following improvements were made to the methodology of Aoki et al. (2016):

1. We increased the number of seismometers used in the analysis from 128 to 168.
2. Aoki et al. (2016) worked with data from earthquakes for which reflection waves are visually detectable, whereas we used all earthquakes greater than M2.0.
3. Aoki et al. (2016) used a constant Q_C value, but we calculated Q_C values for each waveform.
4. We took account of the height of stations when calculating reflection points.
5. We assumed an inclined stratification structure and changed an angle of the inclined structure so that the angle of the estimated S-wave reflector is the same as that of the assumed inclined structure, in order to detect accurate reflection points.

When we changed the inclined angle, we assumed that the strike and dip directions of the reflector were E–W and north, respectively, following Aoki et al. (2016).

Results and discussion

Inclined angle

In this study, we projected relative reflection strengths onto cross sections shown in Figs. 2, 3, 4, and 5. When the relative reflection strength in the grid cell is greater than the average relative reflection strength estimated by coda normalization, the relative reflection strength is greater than 1. We evaluated the accuracy of the relative reflection strength by the number of data points, which is related to the number of rays passing through the grid. The number of data points is computed as the number of samples in waveform envelopes assigned to a grid cell by NMO correction. For example, if an S-wave entered a grid cell vertically, the grid includes about 71 data points, because the sampling frequency of the Manten system is 250 Hz, the vertical grid cell size is 1 km, and the S-wave velocity is assumed to be 3.5 km/s. Aoki et al. (2016) calculated standard errors in each grid cell and found that relative reflection strengths are sufficiently accurate if the number of data points is greater than 10,000. This is equivalent to S-waves entering the grid cell at least 141 times. Therefore, we only discuss results for which the number of data points is greater than 10,000. These ranges are enclosed by blue lines in each figure. Furthermore, we only discuss results obtained below a depth of 20 km because the effect of direct S-waves that could not be removed caused high relative reflection strengths.

Blue stars in each figure indicate hypocenters of DLFs determined by Japan Meteorological Agency (JMA) occurring in this region between 2000 and 2013. The DLFs shown in each figure are located within 5 km of each section. There are five hypocentral regions of DLFs near fault zones where earthquakes of M7 or >M7 class can occur (the Headquarters for Earthquake Research Promotion (HERP) 2003, 2005, 2009) (Fig. 1), and the most active DLF hypocentral area is S1. Aoki et al. (2016) found that the northern edge of the S-wave reflector is close to S1.

Aoki et al. (2016) assumed a horizontal stratification structure and found that the remarkable S-wave reflector was inclined. However, because the inferred reflector is inclined, the deduced reflecting points of the seismic waves and the location of the S-wave reflector possibly differ from reality. Therefore, we assumed an inclined stratification structure of constant inclination, and we changed the angle of inclination to precisely detect the location of the S-wave reflector (Fig. 2). In this study, we define an S-wave reflector as a continuous planar body with relative reflection strengths greater than 1.2. Relative reflection strengths greater than 1.2 are distributed continuously above S2 and S3. This series of high relative reflection strengths may have the same inclined angle.

If an inclined S-wave reflector is continuous, the assumed angle of inclination is regarded as the real angle of inclination when the assumed angle is equal to an inclined angle of the estimated S-wave reflector. Then, the position of the reflector should be determined more accurate. We focused on the S-wave reflector near S1 and varied the assumed angles of inclination in steps of 5° from 0° to 20°. When we assumed 15°, the assumed inclined angle was equal to the inclination of the estimated S-wave reflector. We conclude that the inclined angle of the S-wave reflector near S1 is 15°. We also found that the inclined angle of the S-wave reflector near S2 is 15°. The remaining results reported were obtained when we assumed an inclined angle of 15°. We call the S-wave reflector reported by Katao et al. (2007) and Aoki et al. (2016) "reflector W," and the S-wave reflector that exists on the east side of reflector W, "reflector E." If these S-wave reflectors are stair-shaped, in perspective they may be imaged as inclined at 15°.

We assumed an inclined stratification structure and obtained more detailed results than Aoki et al. (2016). We found that reflector E is situated in an area that Aoki et al. (2016) were unable to image. In this study, we found that

(See figure on next page.)

Fig. 2 Relative reflection strengths of an inclined stratification structure along NS vertical cross section. Reflection strengths take account of inclined angles (0°, 5°, 10°, 15°, and 20°). The color scale and plane locations are shown on the middle left. Blue stars represent hypocenters of deep low-frequency earthquakes (DLFs). Hypocenters occurring within 5 km of each plane are plotted. Black lines represent active faults. The assumed angle of inclination is shown at the upper left-hand side in each panel. Blue lines indicate area in which the number of data points assigned to each grid cell exceeds the threshold value of 10,000. We consider that relative reflection strengths within the blue lines are sufficiently accurate

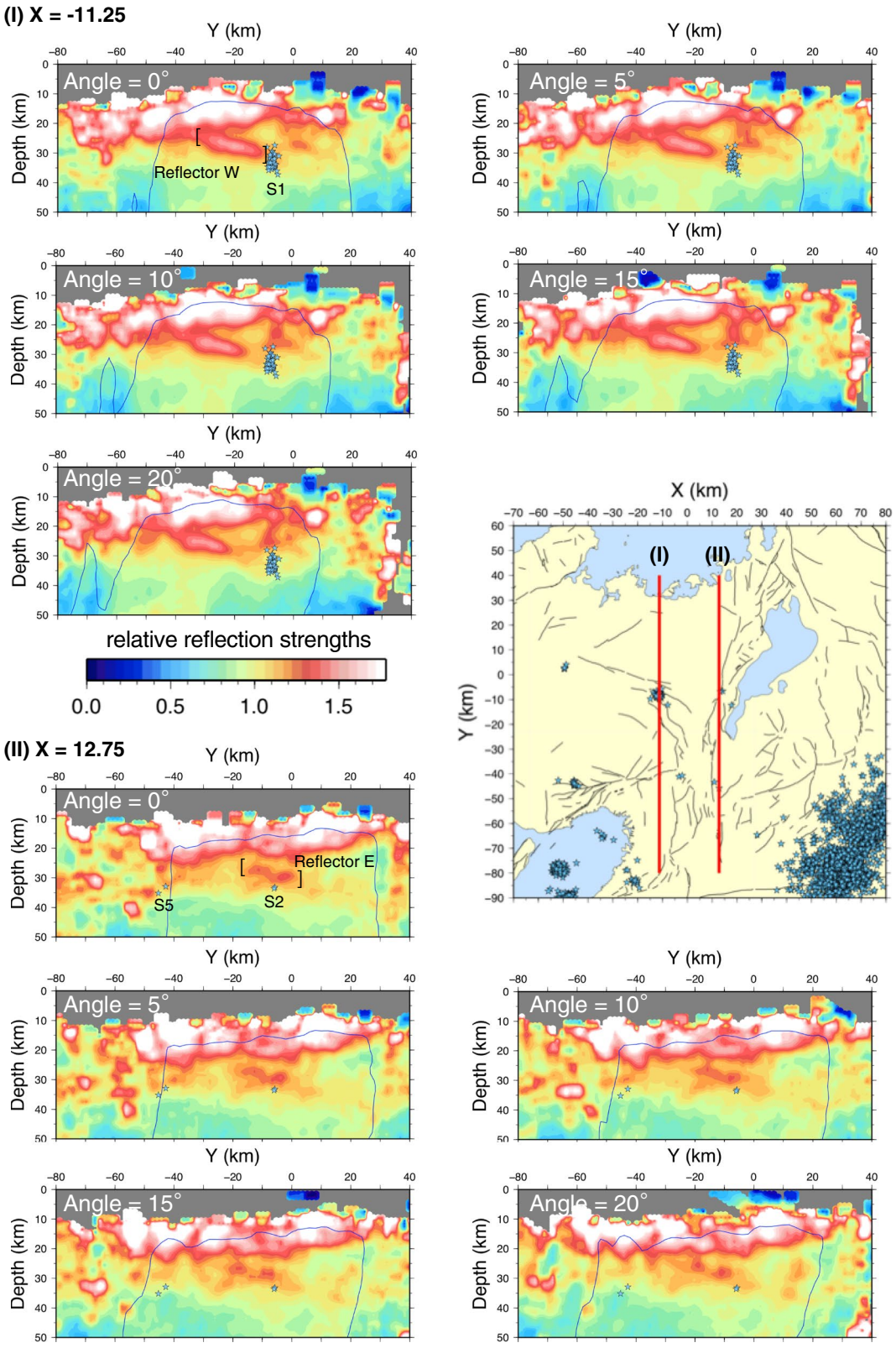
(I) X = -11.25
Y (km)
Depth (km)
Angle = 0°
Reflector W
S1
Angle = 5°
Angle = 10°
Angle = 15°
Angle = 20°
relative reflection strengths
0.0
0.5
1.0
1.5
X (km)
(I)
(II)
Y (km)
(II) X = 12.75
Angle = 0°
Reflector E
S5
S2
Angle = 5°
Angle = 10°
Angle = 15°
Angle = 20°

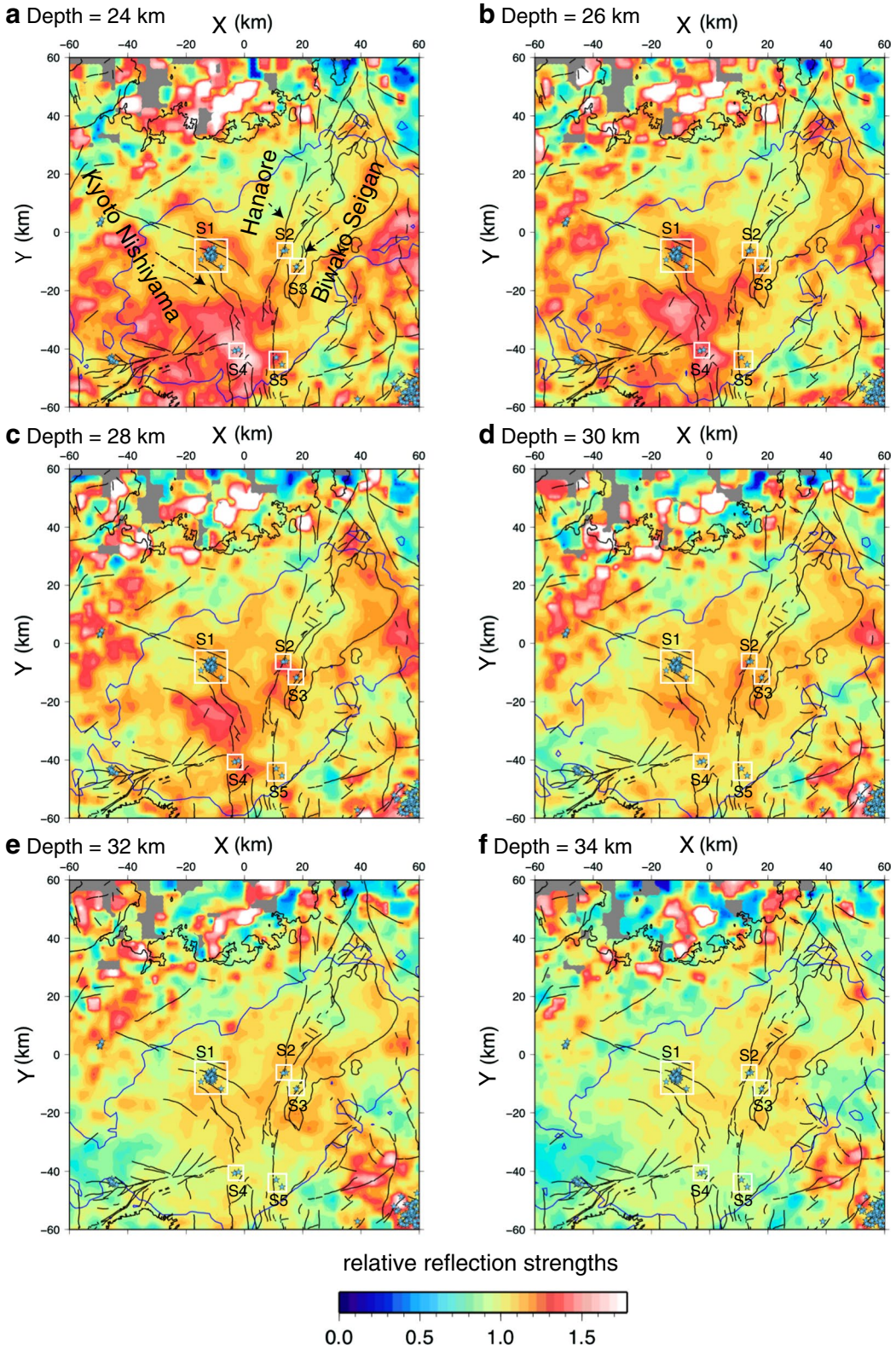

Fig. 3 Relative reflection strengths on horizontal cross section [depth = 24, 26, 28, 30, 32, 34 km]. The blue line shows areas in which there are more than 10,000 samples per grid cell. Black lines represent active faults. White squares represent hypocentral areas projected on the surface [S1, S2, S3, S4, and S5]. Hypocenters of DLFs are plotted regardless of their depth. The names of the fault zones [Kyoto Nishiyama, Hanaore, and Biwako Seigan] are putted near each fault zone

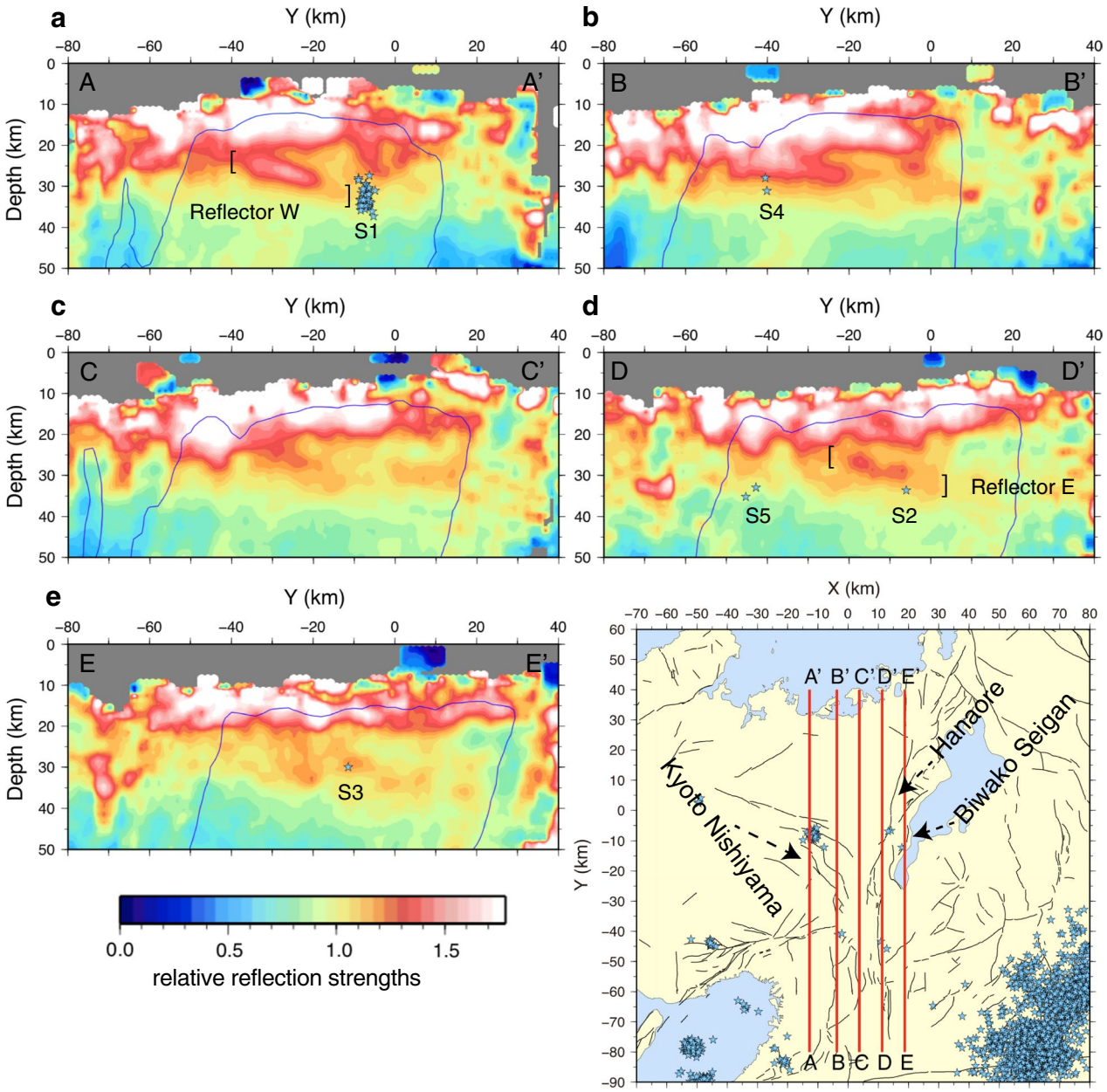

Fig. 4 Relative reflection strengths along NS vertical cross section. The locations of cross sections are shown in the lower right-hand side of the figure. Hypocenters of DLFs occurring within 5 km of each plane are plotted as blue stars. Black lines represent active faults. The assumed angle of inclination is shown at the upper left-hand side of each panel. Blue lines show areas in which the number of data points assigned to each grid cell exceeds 10,000. We consider that relative reflection strengths within blue lines are sufficiently accurate. The names of the fault zones [Kyoto Nishiyama, Hanaore, and Biwako Seigan] are putted near each fault zone in the inset map

reflector W near S1 exists within a range of $Y=-35$ km to $Y=-10$ km and within a depth range of 34–24 km. Furthermore, reflector E near S2 and S3 exists within a range of $Y=-30$ km and $Y=5$ km and within a depth range of 34–24 km.

When we changed the assumed angle of inclination in the vertical cross section of $Y=-11.25$ km, high relative reflection strengths in the shape of a pillar were imaged (Fig. 2(I) angle = 15°). These are probably ghosts that are imaged when changing the assumed angle of inclination.

S-wave reflectors and DLFs

We show results for horizontal sections at depths every 2 km in Fig. 3. The position of the inclined reflector W

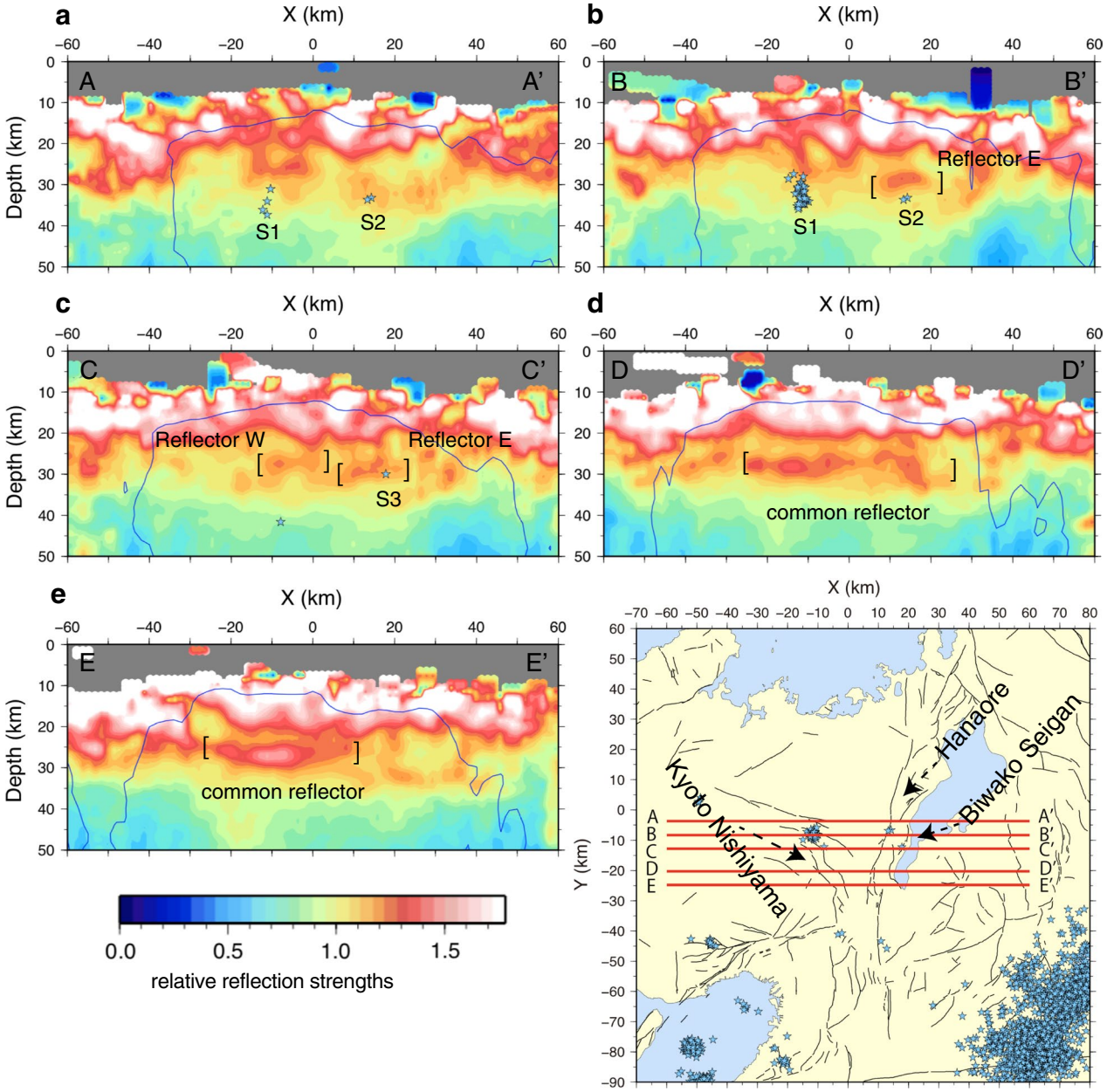

Fig. 5 Relative reflection strengths along EW vertical cross section. The location of cross section is shown in the lower right-hand side of the figure. Blue stars represent hypocenters of DLFs occurring within 5 km of each cross section. Black lines represent active faults. The assumed angle of inclination is shown at the upper left-hand side in each panel. Blue lines show regions in which the number of data points assigned to each grid cell exceeds 10,000. We consider that relative reflection strengths within blue lines are sufficiently accurate. The names of the fault zones [Kyoto Nishiyama, Hanaore, and Biwako Seigan] are putted near each fault zone in the inset map

with its northern edge near S1 is $(X, Y) = (0, -40)$ at a depth of 24 km. The position of reflector W near S1 appears to progress northwestward as it deepens, and the relative reflection strengths decrease below 1.2 near S1. In contrast, the position of reflector E near S2 and S3 progresses in a northeastward as it deepens. The relative reflection strengths also decrease and approach 1.2 near S2 and S3.

Hypocentral areas S1, S2, and S3 and reflector E and reflector W are near active fault zones. S1 and reflector W are near the Kyoto Nishiyama fault zone. Reflector E is near both S2 and S3: S2 is in the vicinity of the

Hanaore fault zone, and S3 is near the Biwako Seigan fault zone (Fig. 3). The inclined reflector W, near S1, and reflector E, near S2 and S3, are imaged in different places in deeper regions, but both S-wave reflectors are imaged and connected at $(X, Y) = (0, -20)$ at a depth of 26 km. In brief, they are imaged as separate S-wave reflectors in deeper regions, but coincide in shallower regions.

We show results for N–S vertical cross sections in Fig. 4. The traverse line shown in Fig. 4a is located near S1. We confirm the inclined S-wave reflector reported by Katao et al. (2007) and Aoki et al. (2016). However, while Aoki et al. (2016) reported that the northern edge of the inclined S-wave reflector with relative reflection strength greater than 1.3 is located within 5 km of S1, we found that it is much further than 10 km from S1. Reflector W, with relative reflection strength between 1.2 and 1.3, extends to S1 at the same angle from the S-wave reflector with relative reflection strength greater than 1.3. In Fig. 4b the same reflector W is confirmed. The traverse line B–B′ is located near S4. Relative reflection strengths are high, but details cannot be resolved because this region overlaps with the area where direct S-waves that cannot be removed cause high relative reflection strengths. In Fig. 4a and b, relative reflection strengths are higher than 1.3 only on the south side of $Y = -20$ km. Reflector W, near S1, is coincident with reflector E near S2 and S3 at $Y = -20$ km. This is confirmed by results in the horizontal section. Relative reflection strengths increase in the place where S-wave reflectors near different hypocentral areas of DLFs are combined.

Figure 4d illustrates reflector E near S2 and S3. The shape of reflector E is not clearer than that of reflector W near S1. S2 is at the northern edge of reflector E. High relative reflection strengths exist near S5. It can also be seen in Fig. 4e relative reflection strengths are high near S3.

We show results for E–W vertical cross sections in Fig. 5. In Fig. 5a, we show that relative reflection strengths near S1 extend in E–W direction, and relative reflection strengths are high near S2. In Fig. 5b, we show that reflector E near S2 and S3 extends in E–W directions. In Fig. 5c–e, we show reflector W near S1. In Fig. 5c, we show that reflector W near S1 spreads from $X = -15$ km to $X = 0$ km, and reflector E near S2 and S3 spreads from $X = 5$ km to $X = 20$ km. Different S-wave reflectors are imaged as a common S-wave reflector on traverse lines D–D′ and E–E′ of the south side from the traverse line C–C′. When we change the position of the traverse line to the south, the depth of the common S-wave reflector becomes shallower.

Mechanism causing DLFs in the study area

Isolated intraplate DLFs occur under the hypocentral area of the 2000 western Tottori earthquake. Tomography of this region (Zhao et al. 2000) suggests that the hypocentral area of DLFs is located at the edge of a low-velocity zone. This low-velocity zone is thought to result from the existence of fluid dehydrated from the slab (Zhao et al. 2000). Ohami and Obara (2002) studied focal mechanisms of DLFs and suggested that the focal mechanism of this DLF indicates a single force source mechanism, which suggests the transport of fluid such as water. They consider that DLFs occur, resulting in fluid pouring into faults.

The hypocenter of DLFs in this study is located near active faults, and the DLFs in the S1 and S3 occur in almost directly above the Moho discontinuity at a depth of 30–35 km in this region (Ueno et al. 2008). Tomography suggests the existence of a low-velocity zone in the lower crust (Nakajima and Hasegawa 2007). From the fact that the Philippine Sea plate is subducting in this region to at least 50 km in depth (Hirose et al. 2008), Nakajima and Hasegawa (2007) considered that this low-velocity zone may imply the existence of fluid dehydrated from the plate in the lower crust. It is possible that the fluid generates DLFs in this region, in a similar way to that under the hypocentral area of the 2000 western Tottori earthquake.

Further evidence of fluid in this region is found in the study of helium isotope ratios in the northern Kinki district, southwestern Japan (Umeda et al. 2007; Sano and Nakajima 2008). ^{3}He is scarce in the Earth's crust, but abundant in the mantle, whereas the situation is reversed for ^{4}He; hence, high helium isotope ratios imply a mantle source for material. Studies of helium isotope ratios (Sano and Nakajima 2008; Umeda et al. 2007) indicate that the helium isotope ratio is high around S3, which indicates the existence of materials passed through the mantle under the hypocenter of S3. The results of tomography and helium isotope ratios may imply the existence of fluid dehydrated from the subducting Philippine Sea plate in the lower crust.

Results of helium isotope ratios and tomography lead us to believe that DLFs that occur in S2 and S3 are related to fluid dehydrated from the subducting Philippine Sea plate. Reflector E near S2 and S3 may correspond to this fluid, because relative reflection strengths are high under the area with a high helium isotope ratio and around the hypocentral area of DLFs (S3). Reflector W near S1 may also be related to the fluid, because reflector W near S1 unites with reflector E near S2 and S3. Fluid may be injected through the DLFs hypocentral area from the mantle to the lower crust. The fact that the isolated DLFs occur in S1, S2, and S3 may imply that fluid is injected

through the hypocentral areas of the DLFs. We consider that the S-wave reflectors may represent the fluid that exists along fractures generated by faulting. However, that physical process has not been investigated in detail. Results suggesting the existence of fluid under the active fault in the lower crust are in accordance with the water-weakened lower crust model proposed by Iio et al. (2002).

Conclusion

We conducted high-resolution reflection analysis, accounting for inclined angles of S-wave reflectors in the northern Kinki district, southwestern Japan. We detected the inclined angle and location of reflector W near S1 as reported in previous studies (Katao et al. 2007; Aoki et al. 2016). We found reflector E near S2 and S3. This reflector has the same angle as reflector W near S1. These S-wave reflectors exist above the Moho discontinuity and appear as different reflectors in deeper regions, but coalesce in shallower regions. According to tomography and helium isotope ratios, we consider that these S-wave reflectors are formed from fluid dehydrated from the Philippine Sea plate. DLFs occur when this fluid is injected through hypocentral areas of DLFs from the mantle to the lower crust.

Abbreviations

M: magnitude; DLF: deep low-frequency earthquake; NKTZ: Niigata–Kobe Tectonic Zone; NMO: normal move-out; JMA: Japan Meteorological Agency; AIST: National Institute of Advanced Industrial Science and Technology; NIED: National Research Institute for Earth and Disaster Resilience; MEXT: Ministry of Education, Culture, Sports, Science, and Technology; HERP: Headquarters for Earthquake Research Promotion.

Authors' contributions

SK carried out the analysis and drafted the manuscript. YI and HK maintained the seismic stations and helped prepare the manuscript. TM, IY, KT, and MS maintained the seismic stations and supervised the data. All authors read and approved the final manuscript.

Acknowledgements

We are thankful to J.Nakajima and two anonymous reviewers for useful comments and suggestions to improve this manuscript. We thank S. Aoki for providing us with the program. We used seismic data from the National Research Institute for Earth Science and Disaster Prevention (NIED), the National Institute of Advanced Industrial Science and Technology (AIST), the Japan Meteorological Agency (JMA) and Kyoto University. This study was partly supported by JSPS KAKENHI Grant Number 26109006. Figures were drawn by GMT (Wessel and Smith 1991).

Competing interests

The authors declare that they have no competing interests.

Availability of data and materials

The data are basically utilized through cooperative studies.

Consent for publication

Not applicable.

Ethics approval and consent to participate

Not applicable.

Funding

This study was partly supported by JSPS KAKENHI Grant Number 26109006.

Publisher's Note

Received: 28 March 2018 Accepted: 10 September 2018
Published online: 19 September 2018

References

Aki K (1980) Attenuation of shear-waves in the lithosphere for frequencies from 0.05 to 25 Hz. Phys Earth Planet Inter 21:50–60

Aoki S, Iio Y, Katao H, Miura T, Yoneda I, Sawada M (2016) Three-dimensional distribution of S wave reflectors in the northern Kinki district, southwestern Japan. Earth Planets Space 68:107. https://doi.org/10.1186/s40623-016-0468-3

Aso N, Ohta K, Ide S (2012) Tectonic, volcanic, and semi-volcanic deep low-frequency earthquakes in western Japan. Tectonophysics 27:40

Doi I, Nishigami K (2007) Three-dimensional distributions of S wave reflectors in the source region of the 2000 Western Tottori Earthquake. Geophys Res Lett 34:L20312

Hirose F, Nakajima J, Hasegawa A (2008) Three-dimensional seismic velocity structure and configuration of the Philippine Sea slab in southwestern Japan estimated by double-difference tomography. J Geophys Res 113:B09315

Iio Y (1996) A possible generating process of the 1995 Southern Hyogo Prefecture Earthquake. Zisin J Seismol Soc Jpn 2(49):103–112 **(in Japanese)**

Iio Y (2011) Development of a seismic observation system in the next generation to install ten thousands stations. Ann Disaster Prev Res Inst Kyoto Univ 54(A):17–24 **(in Japanese)**

Iio Y, Sagiya T, Kobayashi T, Shiozaki I (2002) Water-weakened lower crust and its role in the concentrated deformation in the Japanese Island. Earth Planet Sci Lett 203:245–253

Inamori T, Horiuchi S, Hasegawa A (1992) Location of mid-crustal reflectors by a reflection method using aftershock waveform data in the focal area of the 1984 Western Nagano Prefecture Earthquake. J Phys Earth 40:379–393

Katao H (2002) Seismicity of Tamba region. Chikyu Mon extra 38:42–49 **(in Japanese)**

Katao H, Ito K, Nakao S, Hirose I, Nishimura K, Fukushima M (2007) Seismic survey on the deep reflector beneath the Tamba Plateau. Ann Disaster Prev Res Inst Kyoto Univ 50(B):297–302 **(in Japanese)**

Miura T, Iio Y, Katao H, Nakao S, Yoneda I, Fujita Y, Kondo K, Nishimura K, Sawada M, Tada M, Hirano N, Yamazaki T, Tomisaka K, Tatsumi K, Kamo M, Shibutani T, Ohmi S, Kano Y (2010) Temporary seismic observation in the Northern Kinki district. Ann Disaster Prev Res Inst Kyoto Univ 53(B):203–212 **(in Japanese)**

Nakajima J, Hasegawa A (2007) Deep crustal structure along the Niigata–Kobe Tectonic Zone, Japan: its origin and segmentation. Earth Planets Space 59:e5. https://doi.org/10.1186/BF03352677

Obara K (2002) Nonvolcanic deep tremor associated with subduction in southwest Japan. Science 296:1679–1681

Ohami S, Obara K (2002) Deep low-frequency earthquakes beneath the focal region of the Mw 6.7 2000 Western Tottori earthquake. Geophys Res Lett 29:54-1–54-4

Sagiya T, Miyazaki S, Tada T (2000) Continuous GPS array and present-day crustal determined of Japan. Pure Appl Geophys 157:2303–2322

Sano Y, Nakajima J (2008) Geographical distribution of 3He/4He ratios and seismic tomography in Japan. Geochem J 42:51–60

The Headquarters for Earthquake Research Promotion (2003) The long-term evaluation of the Mikata-Hanaore fault zone. https://www.jishin.go.jp/main/chousa/katsudansou_pdf/78_mitoke_kyoto-nishiyama.pdf. Accessed 20 Mar 2018

The Headquarters for Earthquake Research Promotion (2005) The long-term evaluation of the Mitoke-Kyoto Nishiyama fault zone. https://www.jishin.go.jp/regional_seismicity/rs_katsudanso/f078_mitoke_kyoto-nishiyama/. Accessed 20 Mar 2018

The Headquarters for Earthquake Research Promotion (2009) The long-term evaluation of the Biwako Seigan fault zone. https://www.jishin.go.jp/main/chousa/katsudansou_pdf/65_biwako-seigan_2.pdf. Accessed 20 Mar 2018

Ueno H, Hatakeyama S, Aketagawa T, Fuasaki J, Hamada N (2002) Improvement of hypocenter determination procedures in the Japan Meteorological Agency. Q J Seismol 65:123–134 **(in Japanese)**

Ueno T, Shibutani T, Ito K (2008) Configuration of the continental Moho and Philippine Sea Slab in Southwest Japan derived from receiver function analysis: relation to subcrustal earthquakes. Bull Seismol Soc Am 98(5):2416–2427

Umeda K, Sakagawa Y, Ninomiya A, Asamori K (2007) Relationship between helium isotopes and heat flux from hot springs in a non-volcanic region, Kii Peninsula, southwest Japan. Geophys Res Lett 34:L05310

Wessel P, Smith WHF (1991) Free software helps map and display data. EOS Trans AGU 72:441

Zhao D, Ochi F, Hasegawa A, Yamamoto. (2000) Evidence for the location and cause of large crustal earthquakes in Japan. J Geophys Res 105:13579–13594